Physica D 278–279 (2014) 13–30

Contents lists available at ScienceDirect

Physica D

journal homepage: www.elsevier.com/locate/physd

Modeling selective local interactions with memory: Motion on a 2D lattice

Daniel Weinberg, Doron Levy *

Department of Mathematics and Center for Scientific Computation and Mathematical Modeling (CSCAMM), University of Maryland, College Park, MD 20742, USA

HIGHLIGHTS

- A 2D ODE model for local interactions between cells on a periodic lattice.
- Model includes a selective motion toward a neighboring particle.
- Simulates and replicates observed experimentally patterns of motion.

ARTICLE INFO

Article history:
Received 28 June 2013
Received in revised form
2 January 2014
Accepted 8 April 2014
Available online 13 April 2014
Communicated by T. Wanner

Keywords:
Agent-based models
Group dynamics
Reaction–diffusion master equation
Collective motion

ABSTRACT

We consider a system of particles that simultaneously move on a two-dimensional periodic lattice at discrete times steps. Particles remember their last direction of movement and may either choose to continue moving in this direction, remain stationary, or move toward one of their neighbors. The form of motion is chosen based on predetermined stationary probabilities. Simulations of this model reveal a connection between these probabilities and the emerging patterns and size of aggregates. In addition, we develop a reaction–diffusion master equation from which we derive a system of ODEs describing the dynamics of the particles on the lattice. Simulations demonstrate that solutions of the ODEs may replicate the aggregation patterns produced by the stochastic particle model. We investigate conditions on the parameters that influence the locations at which particles prefer to aggregate. This work is a two-dimensional generalization of Galante and Levy (2012), in which the corresponding one-dimensional problem was studied.

1. Introduction

In a series of recent works [1–6] we developed mathematical models for describing various aspects of the motion of the cyanobacteria *Synechocystis* sp., which are coccoidal bacteria that move towards light, a motion known as phototaxis. As a result of this motion, finger-like appendages form on a large scale [7,8]. In contrast, in regions of low and medium density, cells follow a quasi-random pattern of motion in which small aggregates form, yet bacteria may still move in various directions without any observable bias in the direction of the light source.

This quasi-random motion in regions of low-density was the focus of our works in [2,3] in which we developed mathematical models to describe the emerging patterns of motion. Our approach was to construct stochastic particle models in which we considered individual particles that move according to a prescribed set of rules at discrete time steps. The rules of motion allowed the particles to persist in their previous direction of motion, become stationary or start moving if already stationary, and change the direction of their motion. When a particle changes its direction of motion, it can only choose to move towards one of its neighbors. Particles can detect their neighbors within a given detection range. These models generated patterns of motion that qualitatively agree with the experimental data.

In order to gain a better understanding of the mathematical model, we developed a one-dimensional version of our stochastic model from [2,3], in which particles were constrained to move on a one-dimensional lattice [1]. In this context, it became possible to develop a system of ODEs that quantify the expected number of particles at each position, following the method outlined in [9]. The results of the stochastic model agreed in many cases with the results of the deterministic model, depending on the choice of parameters. In addition, randomly chosen initial conditions in the deterministic model led to the formation of aggregates in most cases.

* Corresponding author.
E-mail addresses: dweinberg@cscamm.umd.edu (D. Weinberg), dlevy@math.umd.edu (D. Levy).

http://dx.doi.org/10.1016/j.physd.2014.04.001
0167-2789/

In this paper, we generalize the one-dimensional model from [1] to a motion on a two-dimensional lattice and use numerical simulations to study the emerging patterns. Similarly to [1], our study starts with a stochastic particle system and proceeds with a system of ODEs that capture the averaged behavior of the discrete system.

It is important to note that this study is an example of a flocking model. Mathematical models of flocking phenomena have became very popular in recent years, most of which intend to describe a process in which self-propelled individual organisms act collectively. Examples for such models include flocking models for fish [10–13], birds [14,15], and insects [16,17], among many others. Various mechanisms have been proposed in the literature for changing the direction of motion. In [15], Reynolds models a flock of birds using the rules of collision avoidance, velocity matching, and attraction within a certain radius. Vicsek et al. propose a simple model where the only rule is for each individual to assume the average direction of its neighbors, with some random perturbation [18]. In the model of Couzin et al., particles have a zone of repulsion, a zone of orientation in which they match their neighbors' directions, and a zone of attraction [19]. The Cucker–Smale model proposes that a bird changes its velocity at each time step by adding a weighted average of the differences between its velocity and those of other birds [14]. In contrast, our approach requires a particle to move towards *one* of its neighbors.

The structure of this paper is as follows. After reviewing the one-dimensional models in Section 2, we introduce the two-dimensional stochastic particle model in Section 3.1. Multiple simulations of the stochastic particle model are conducted in Section 3.2. We observe the formation of horizontal and vertical aggregates whose lengths depend upon the choice of parameters.

In Section 4.1, we derive a system of ODEs that captures the averaged behavior of the stochastic particle model. The correspondence between the stochastic particle model and the ODEs model is demonstrated in Section 4.2. The ODEs system also results in the formation of aggregates, at least when the model parameters are confined to a certain range. Concluding remarks are provided in Section 5.

2. Review of the one-dimensional models

We start by reviewing the one-dimensional model from [1]. Consider a set of N particles that occupy the k vertices of a one-dimensional lattice. There are no restrictions on the number of particles that can occupy each bin. We fix a detection radius $D \geq 1$ which determines how far away a particle can detect neighboring particles. At every discrete time-step, each particle can either

(i) persist in its last direction with probability a,
(ii) become stationary with probability b,
(iii) choose to move towards another particle within its detection radius with neighbor-weighted probabilities.

If we denote the position of the nth particle at time $t \in \mathbb{N}$ by $x_n(t)$ and the direction of last movement by $p_n(t) \in \{\pm 1\}$, the rules of motion are

$$x_n(t+1) - x_n(t) = \begin{cases} p_n(t), & \text{w.p. } a, \\ 0, & \text{w.p. } b, \\ 1, & \text{w.p. } (1-a-b)\dfrac{\nu_n^r(t)}{\nu_n(t)}, \\ -1, & \text{w.p. } (1-a-b)\dfrac{\nu_n^l(t)}{\nu_n(t)}, \end{cases} \tag{1}$$

where $\nu_n^r(t)$ and $\nu_n^l(t)$ denote the number of particles at time t that are positioned within a neighborhood of size D centered at the particle n to the right and to the left, respectively. The sum of these two quantities is denoted by $\nu_n = \nu_n^r + \nu_n^l$. Particles that are located at the same position as particle n are excluded from this sum.

Note that these rules should be augmented with rules for motion on the boundary. A simple choice is of a periodic lattice. By doing so, we have a discrete-time Markov process in which the state at each time consists of the positions of the particles as well as the directions of their last movement. Other types of boundary conditions can be used.

The process is difficult to analyze except by simulation, hence we develop in [1] a reaction–diffusion master equation (RDME) that describes how the probabilities of all of the possible states of the systems change in time. The state of the system at any time can be defined by the vectors $\{\vec{r}, \vec{l}, \vec{r^s}, \vec{l^s}\}$, which record the number of right-moving, left-moving, right-moving but currently stationary, and left-moving stationary particles at each position. Define the probability density function $P(\vec{r}, \vec{l}, \vec{r^s}, \vec{l^s}, t)$ which describes the chance of the system being in a certain state at time t. In this case, the RDME can be described by

$$\begin{aligned} &\frac{\partial P}{\partial t}(\vec{r}, \vec{l}, \vec{r^s}, \vec{l^s}, t) \\ &= \sum_{i=1}^{k} [(\text{Probability that the state is entered by a particle} \\ &\qquad \text{in bin } i \text{ moving right}) \\ &\qquad - (\text{Probability the state is exited by a particle in bin } i \\ &\qquad \text{moving right})] \\ &\qquad + \sum_{i=1}^{k} [(\text{Probability the state is entered by a particle} \\ &\qquad \text{in bin } i \text{ moving left}) \\ &\qquad - (\text{Probability the state is exited by a particle in bin } i \\ &\qquad \text{moving left})] \\ &\qquad + \sum_{i=1}^{k} [(\text{Probability the state is entered by a particle} \\ &\qquad \text{in bin } i \text{ becoming stationary}) \\ &\qquad - (\text{Probability the state is exited by a particle} \\ &\qquad \text{in bin } i \text{ becoming stationary})]. \end{aligned} \tag{2}$$

Using the explicit forms of the expressions in (2), we derive ODEs for the expected number of each type of particle in each bin. For example, multiplying (2) by r_i, summing over all possible states, and switching the order of differentiation and summation results in an ODE for the expected number of right-moving particles in bin i. For more details, we refer to [1]. The derivation is described in more detail for the two-dimensional case in Section 4. The resulting system is

$$\begin{aligned} \frac{dR_i}{dt} &= a(R_{i-1} + R_{i-1}^s) + \left\langle n_{i-1} c_{i-1}^r \right\rangle - R_i, \\ \frac{dR_i^s}{dt} &= bR_i - (1-b)R_i^s, \\ \frac{dL_i}{dt} &= a(L_{i+1} - L_{i+1}^s) + \left\langle n_{i+1} c_{i+1}^l \right\rangle - L_i, \\ \frac{dL_i^s}{dt} &= bL_i - (1-b)L_i^s. \end{aligned} \tag{3}$$

Here, n_i corresponds to the total number of particles in bin i, and $\langle x \rangle$ is the expected value of x. The first equation in (3) corresponds to right moving particles in bin i, $R_i(t)$. This population consists of right-moving and stationary particles from bin $i-1$ that persist

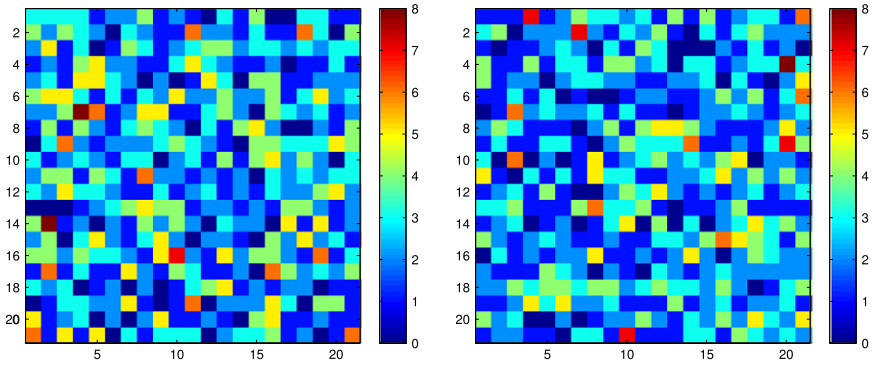

(a) Left-moving particles.

(b) Right-moving particles.

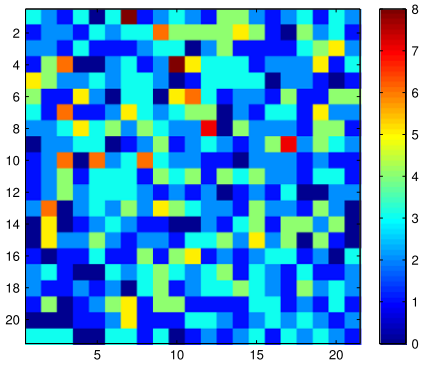

(c) Upward-moving particles.

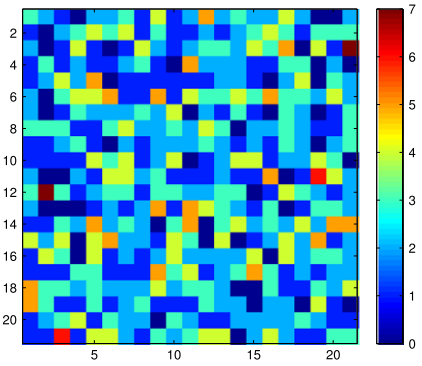

(d) Downward-moving particles.

Fig. 1. Initial configurations for the discrete model. 4000 particles are uniformly placed on a 21×21 grid and are assigned memory (their last direction of motion). The number of particles in every grid-point is shown based on their assigned memory.

into bin i, and particles in bin $i-1$ moving to the right with a neighbor-weighted probability c^r_{i-1}. All right-moving particles leave the system at every time step, either by persisting in their motion to the right, becoming stationary, or choosing to move toward a neighboring bin. The second equation in (3) corresponds to right-stationary particles R^s_i. These consist of particles in R_i that become stationary with stopping probability b, and accounting for particles that leave the stationary state with probability $1-b$. Similar expressions are given by equations three and four in (3) for the left-moving and the left-stationary particles. In practice, in order to simulate the system (3), the expected values of the products are replaced by the products of the expected values.

3. A two-dimensional stochastic particle model

3.1. Model formulation

Assume that N particles are located on the vertices of a $k \times k$ periodic lattice. As in the one-dimensional model, we assume that particles remember their previous direction of movement and can either continue in that direction, choose a new direction, or remain stationary. The detection radius D can be generalized to 2-D by counting the particles within a Euclidean distance of D. To simplify the calculations, we fix the detection radius to be 1 so that particles can only detect only adjacent particles.

We denote the number of particles detected by the nth particle to the left, right, up, and down at time t by $\nu^l_n(t)$, $\nu^r_n(t)$, $\nu^u_n(t)$, and $\nu^d_n(t)$, respectively, with $\nu_n = \nu^l_n + \nu^r_n + \nu^u_n + \nu^d_n$. Let $x_n(t)$ be the position of the nth particle on the lattice with respect to some arbitrary origin at time t. Let a be the probability of persistence and b the probability of becoming or remaining stationary. Finally, let $p_n(t)$ be the vector representing the last direction of movement for particle n. The resulting rules of motion are

$$x_n(t+1) - x_n(t) = \begin{cases} p_n(t), & \text{w.p. } a, \\ 0, & \text{w.p. } b, \\ (1,0), & \text{w.p. } (1-a-b)\dfrac{\nu^r_n(t)}{\nu_n(t)}, \\ (-1,0), & \text{w.p. } (1-a-b)\dfrac{\nu^l_n(t)}{\nu_n(t)}, \\ (0,1), & \text{w.p. } (1-a-b)\dfrac{\nu^u_n(t)}{\nu_n(t)}, \\ (0,-1), & \text{w.p. } (1-a-b)\dfrac{\nu^d_n(t)}{\nu_n(t)}. \end{cases} \tag{4}$$

If a particle has no neighbors, $\nu_n = 0$, then we choose to increase the probability of particle n becoming stationary to $1-a$.

3.2. Simulations of the Stochastic model

All discrete simulations are conducted using the NetLogo multi-agent programable modeling environment (http://ccl.northwestern.edu/netlogo). We start by uniformly distributing 4000 particles on a 21×21 grid. Each particle is assigned a memory in the form of a last direction of motion (left, right, up or down) with equal probabilities. The initial distribution of particles with their associated memories is shown in Fig. 1. We use there initial conditions for all simulations on the 21×21 grid.

The initial configuration is then advanced in time until a final time $t = 1500$ with different values of the parameters. Figs. 2–6 show snapshots of the simulation for a persistence probability $a \in \{0.1, 0.2, 0.3, 0.4, 0.5\}$ in which the probability to remain

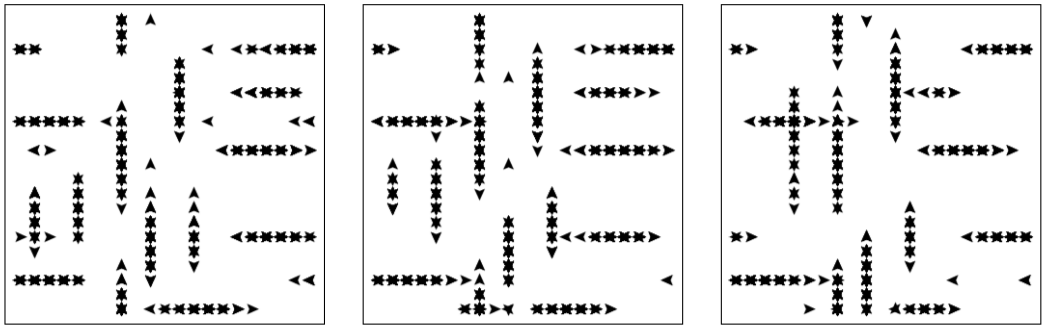

(a) $t = 250$. (b) $t = 500$. (c) $t = 750$.

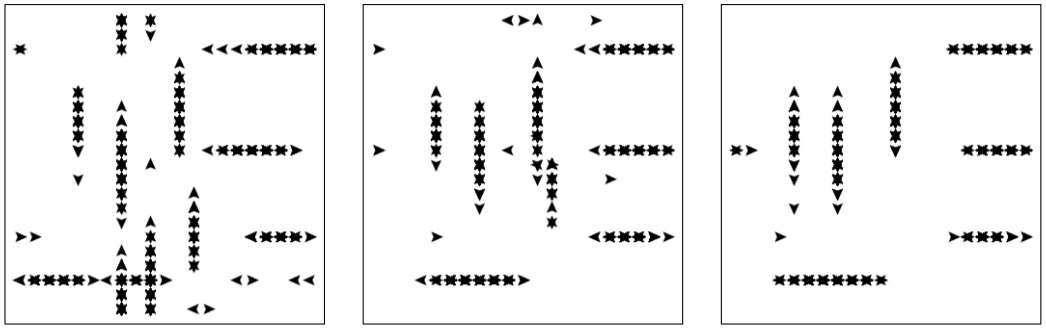

(d) $t = 1000$. (e) $t = 1250$. (f) $t = 1500$.

Fig. 2. Snapshots of the discrete model with $a = 0.1$, $b = 0$. Initially, 4000 particles are randomly placed on a 21×21 grid and given a last direction. The arrows indicate the direction of movement. Each bin may have more than one particle.

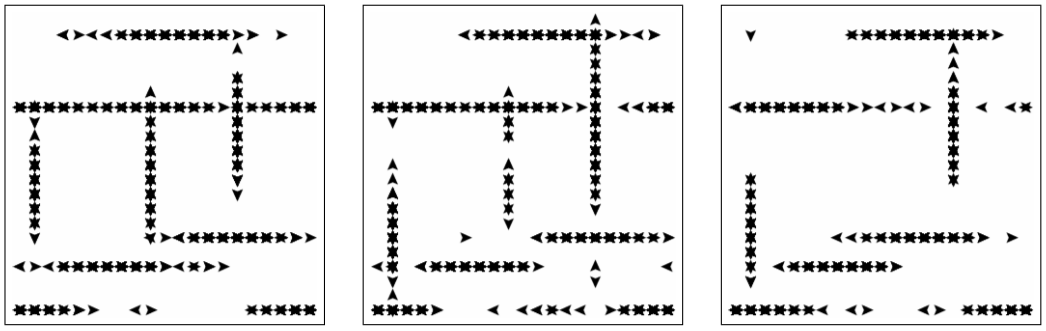

(a) $t = 250$. (b) $t = 500$. (c) $t = 750$.

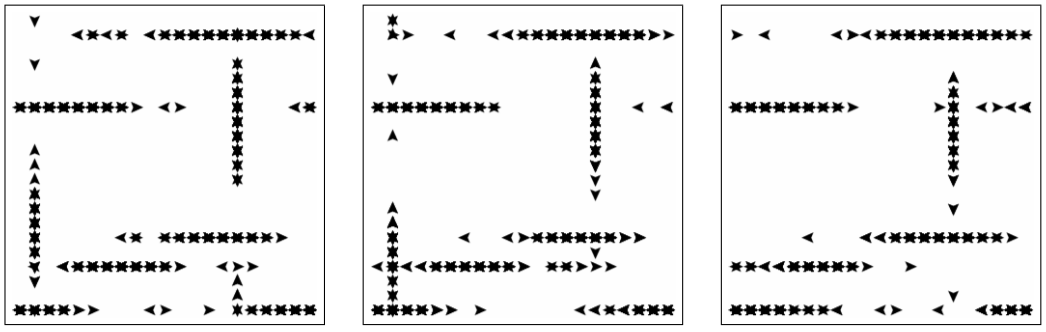

(d) $t = 1000$. (e) $t = 1250$. (f) $t = 1500$.

Fig. 3. Snapshots of the discrete model with $a = 0.2$, $b = 0$.

stationary is set as $b = 0$. In these figures, arrows indicate the direction of movement of particles that are located in any given bin. Bins with no arrows have no particles in them. Each bin may have more than one particle, and hence the total number of arrows in all figures is less than the number of particles (which is 4000).

We define an aggregate as a group of particles occupying horizontally or vertically adjacent bins traveling in the same or opposite directions. In all figures, we see that the particles form horizontal and/or vertical aggregates, which coalesce into fewer aggregates as time elapses. As the value of the persistence

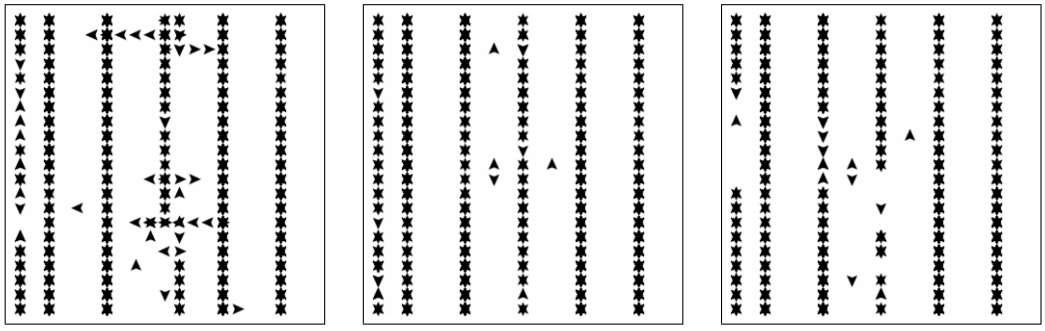

(a) $t = 250$. (b) $t = 500$. (c) $t = 750$.

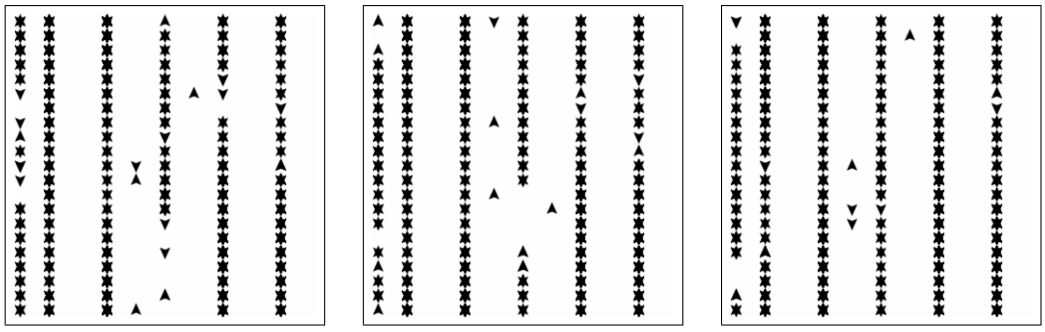

(d) $t = 1000$. (e) $t = 1250$. (f) $t = 1500$.

Fig. 4. Snapshots of the discrete model with $a = 0.3$, $b = 0$.

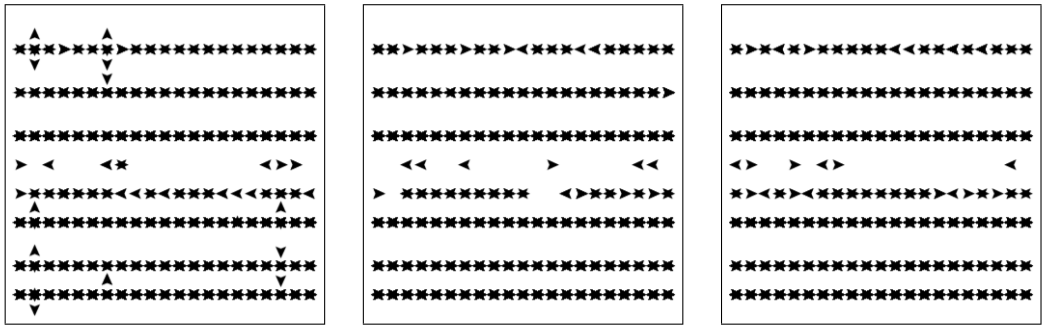

(a) $t = 250$. (b) $t = 500$. (c) $t = 750$.

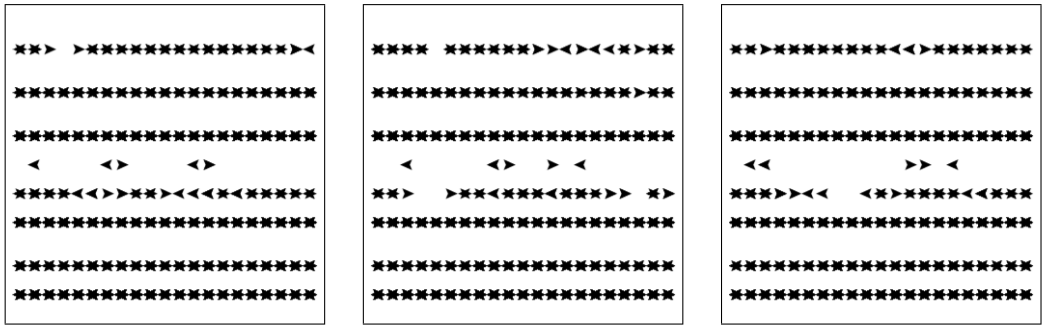

(d) $t = 1000$. (e) $t = 1250$. (f) $t = 1500$.

Fig. 5. Snapshots of the discrete model with $a = 0.4$, $b = 0$.

probability a increases, the length of the aggregates seems to increase. For example, when $a = 0.1$, the average length of the aggregates (ignoring insignificant ones) is approximately 8, while for $a = 0.2$, the average length of the aggregates is approximately 12. When $a = 0.3$ (Fig. 4), the limit aggregates span the entire length of the grid. In general, the average length of significant aggregates does not appear to change significantly after an initial transient period. The length of an aggregate can only increase if an end particle moves away from its neighboring particles, which occurs with probability a when it is facing away from the aggregates. This

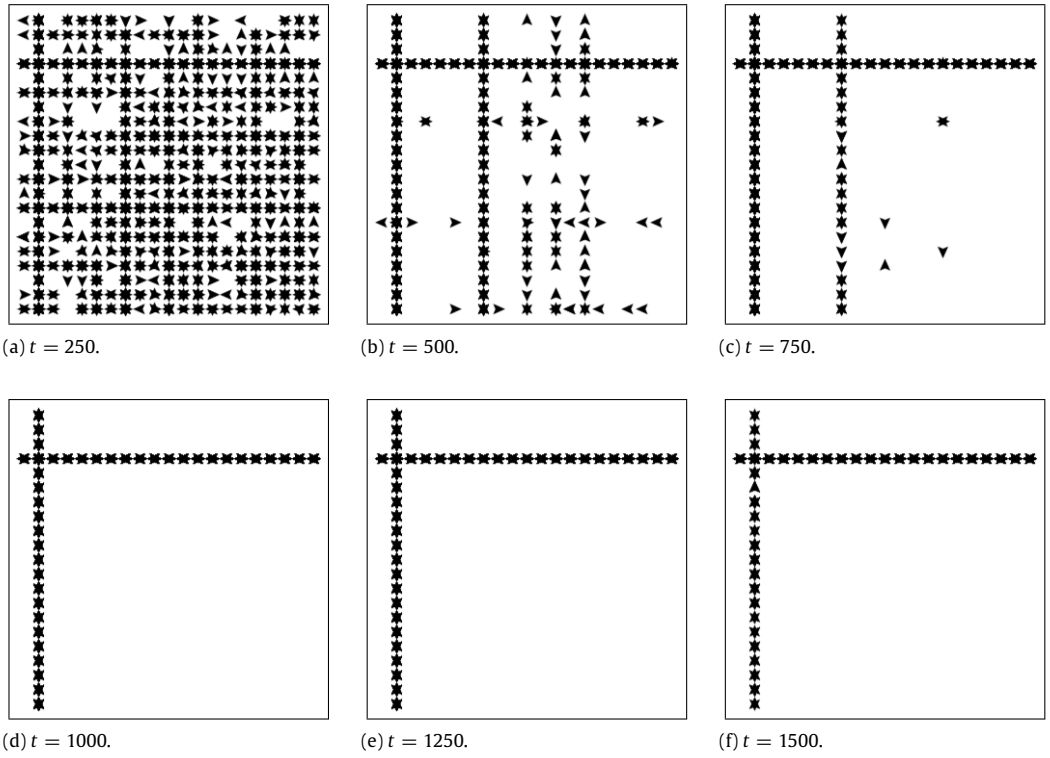

(a) $t = 250$. (b) $t = 500$. (c) $t = 750$.

(d) $t = 1000$. (e) $t = 1250$. (f) $t = 1500$.

Fig. 6. Snapshots of the discrete model with $a = 0.5, b = 0$.

increase in length can only be maintained if a significant number of other particles also move to the new endpoint; however, it is much more likely that the new endpoint will move back to its previous position when a is small, so the aggregates length remains unchanged.

When the persistence probability is $a = 0.5$ (Fig. 6), aggregates are very slow to form. This is due to the high probability of particles continuing their last movement, as opposed to moving towards other particles. At large times, we are left with two long aggregates: one horizontal and one vertical. They eventually coalesce into a single long aggregate.

We note that since we assume a constant nonzero probability of continuing in the same direction, the system is never in steady state and, in particular, stable length-one aggregates do not form. If we set both parameters to 0 for our current initial conditions, the system quickly enters a steady state with only aggregates of length two (Fig. 7). Aggregates of length one are possible if, for example, all particles start in the same bin.

We now investigate the impact of the probability of remaining stationary, b, on the emerging dynamics. We use the same initial configuration given by Fig. 1, fix the persistence probability as $a = 0.3$, and vary $b \in \{0.1, 0.2, 0.3, 0.4, 0.5\}$. The results of these simulations are shown in Figs. 8–12.

Most of these figures are similar: many long aggregates, both horizontal and vertical, form quickly. As time elapses, they coalesce into fewer aggregates, which are all either only horizontal or vertical. Most aggregates span the entire grid, but we can also get smaller aggregates as in Figs. 8 and 11. As b increases, it takes longer for significant aggregates to form. This makes sense since a particle is more likely to remain stationary. When we continue the simulation past $t = 1500$, we are eventually left with purely horizontal or vertical aggregates, though the exact number varies. These results are not shown for the sake of brevity. We hypothesize that this will always be true for any initial conditions as long as the parameters are large enough, though how big the parameters need to be is dependent on grid size and number of particles. For the parameter choice $a = 0.1, b = 0$, a longer time simulation ($t = 5000$) still shows aggregates in both directions (Fig. 13).

It is important to note that since the model is stochastic, the outcomes for a given initial configuration is not unique. This is demonstrated in Fig. 14 in which we show different results that are obtained at $t = 1500$ for the same initial conditions shown in Fig. 1. In most cases (Fig. 14(a), (c)–(f)), purely horizontal or vertical aggregates are all that remain. In Fig. 14(b), however, we have both horizontal and vertical aggregates that will coalesce if we wait sufficiently long.

4. An ODEs model

4.1. Model derivation

Since simulating a large number of particles on a large grid is computationally intensive, we derive a system of ODEs to capture the mean number of particles in each bin. Let $P = P(\Psi)$ denote the probability of the system being in a given state $\Psi = (r, l, u, d, r^s, l^s, u^s, d^s)$. Here, r is a $k \times k$ matrix that denotes the number of right-moving particles at every node. Similarly, (l, u, d) are matrices that correspond to the number of left, up, and down-moving particles in every node. The variables with a superscript "s" correspond to the stationary particles and are divided into four groups based on the last direction of motion that brought them to their present location, a direction which they remember.

Generally, the evolution of the probability is given by:

$$\frac{\partial P}{\partial t}(\Psi, t) = \sum_{i,j,\mathcal{D}} \left[\begin{pmatrix} \text{Probability that a particle moves out of node } (i,j) \\ \text{in direction } \mathcal{D} \text{ to enter the state } \{\Psi, t\} \end{pmatrix} \right.$$

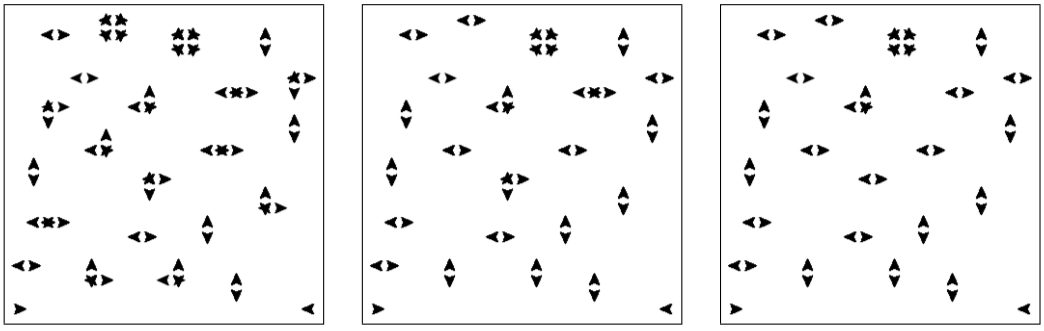

(a) $t = 100$. (b) $t = 200$. (c) $t = 300$.

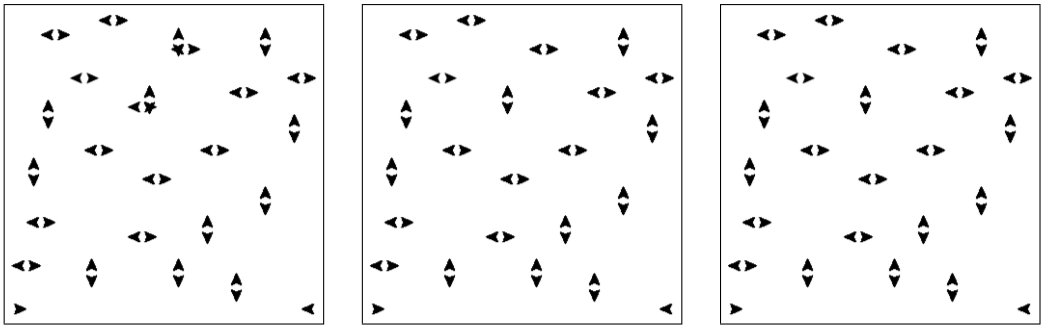

(d) $t = 400$. (e) $t = 500$. (f) $t = 600$.

Fig. 7. Snapshots of the discrete model with $a = 0$, $b = 0$.

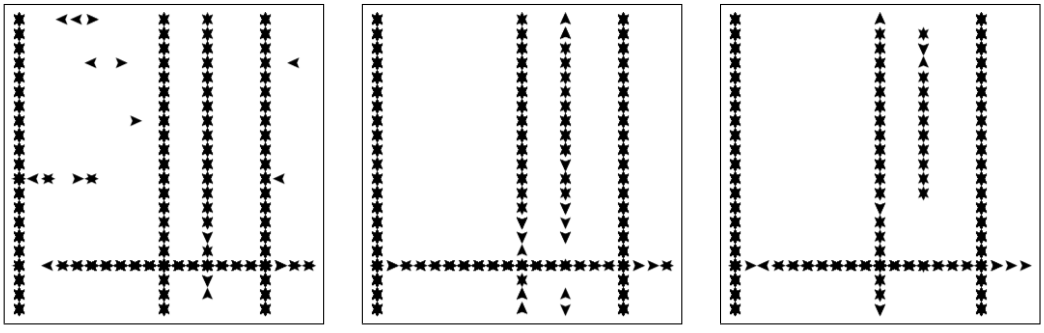

(a) $t = 250$. (b) $t = 500$. (c) $t = 750$.

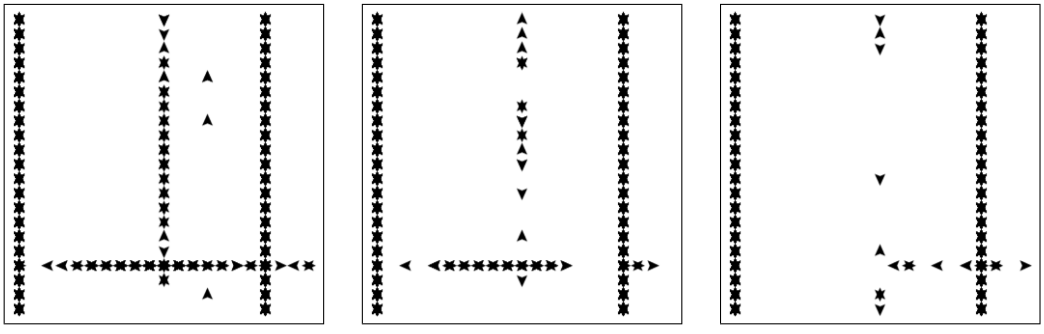

(d) $t = 1000$. (e) $t = 1250$. (f) $t = 1500$.

Fig. 8. Snapshots of the discrete model with $a = 0.3$, $b = 0.1$.

$$- \left(\begin{array}{c} \text{Probability that a particle moves out of node } (i,j) \\ \text{in direction } \mathcal{D} \text{ to leave the state } \{\Psi, t\} \end{array} \right) \Bigg] + \sum_{i,j} \left(\begin{array}{c} \text{Probability that a particle in node } (i,j) \text{ becomes} \\ \text{stationary to enter or leave the state } \{\Psi, t\} \end{array} \right). \quad (5)$$

The summation over the direction $\mathcal{D}$ corresponds to a summation in all directions: left, right, up, and down.

Let $\tilde{P}(.,.)$ denote the probability P of a state with a specified change. For example, $\tilde{P}(r_{ij}+1, r_{i+1,j}-1)$ is P with the number of right-moving particles at node (i,j), r_{ij}, increased by one, and the number of right-moving particles at $(i+1,j)$ decreased by one.

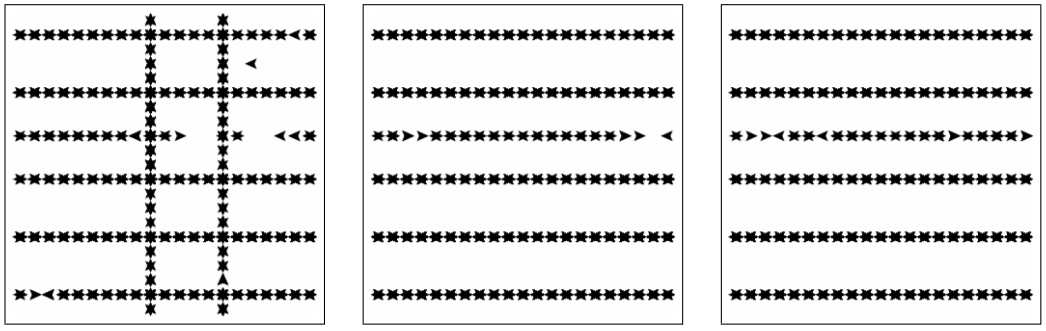

(a) $t = 250$. (b) $t = 500$. (c) $t = 750$.

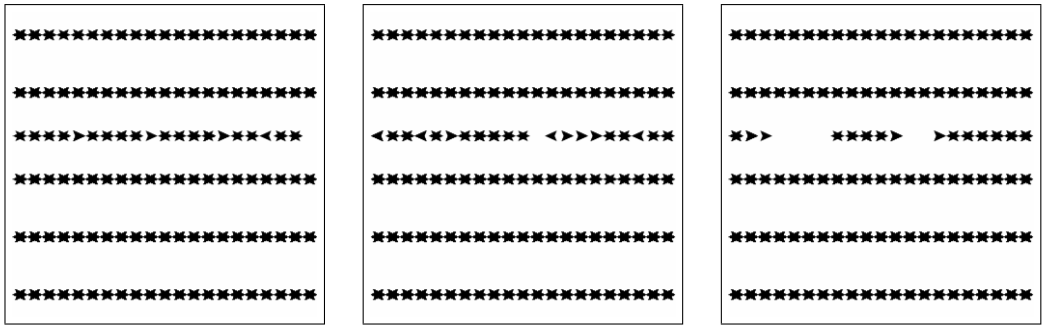

(d) $t = 1000$. (e) $t = 1250$. (f) $t = 1500$.

Fig. 9. Snapshots of the discrete model with $a = 0.3$, $b = 0.2$.

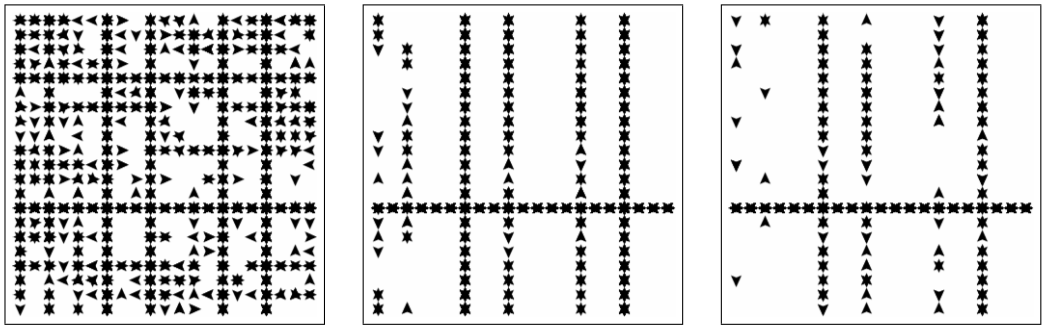

(a) $t = 250$. (b) $t = 500$. (c) $t = 750$.

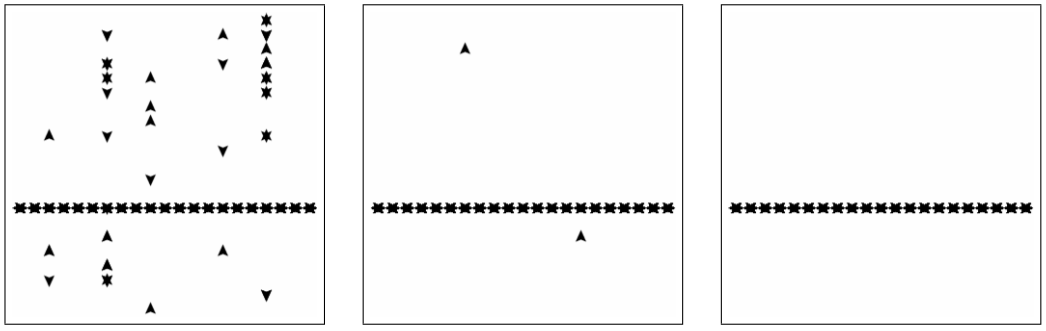

(d) $t = 1000$. (e) $t = 1250$. (f) $t = 1500$.

Fig. 10. Snapshots of the discrete model with $a = 0.3$, $b = 0.3$.

Note that $\tilde{P}$ is not a function; it is notation that greatly simplifies the derivation below. We recall that v_{ij}^r denotes the number of particles within the detection range to the right of node (i, j), and that v_{ij} is the total number of particles within the detection range in all directions surrounding node (i, j). Accordingly, we define

$$c_{ij}^r = (1 - a - b)\frac{v_{ij}^r}{v_{ij}},$$

as the probability that a particle at (i, j) chooses to move to the right. In addition, we define the probability

$$\overline{c_{ij}^r} = (1 - a - b)\frac{v_{ij}^r - 1}{v_{ij} - 1}.$$

$\overline{c_{ij}^r}$ is the probability a particle at (i, j) chooses to move to the right when the number of particles to the right of (i, j) within the

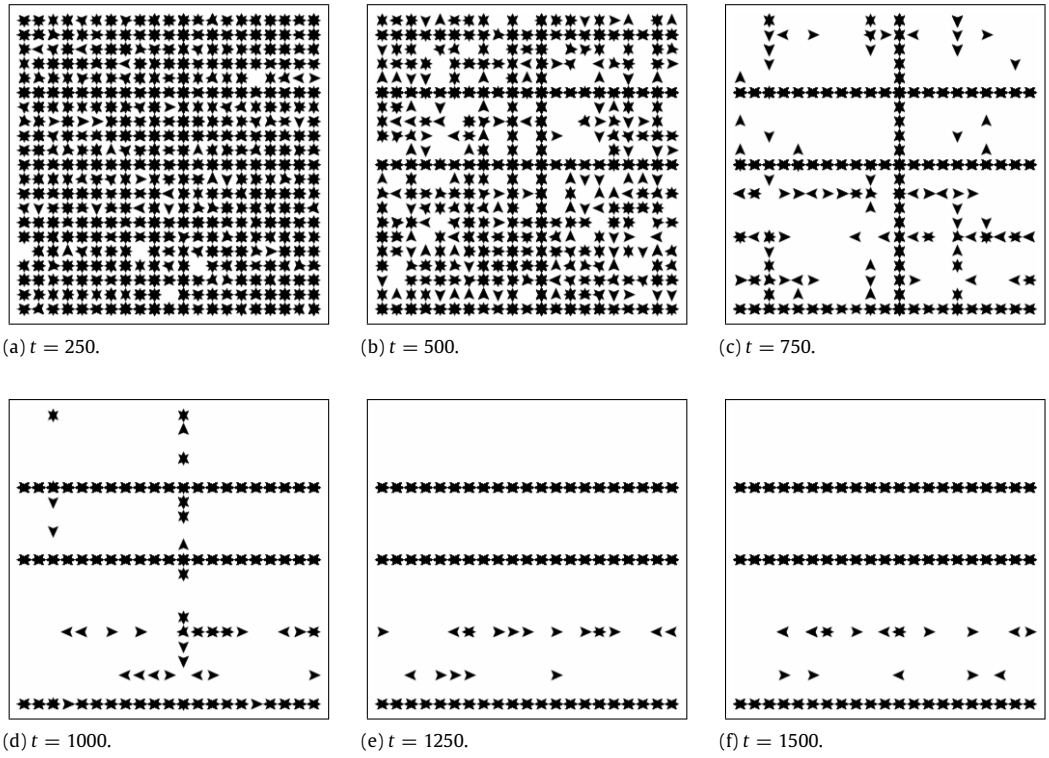

(a) $t = 250$. (b) $t = 500$. (c) $t = 750$.

(d) $t = 1000$. (e) $t = 1250$. (f) $t = 1500$.

Fig. 11. Snapshots of the discrete model with $a = 0.3, b = 0.4$.

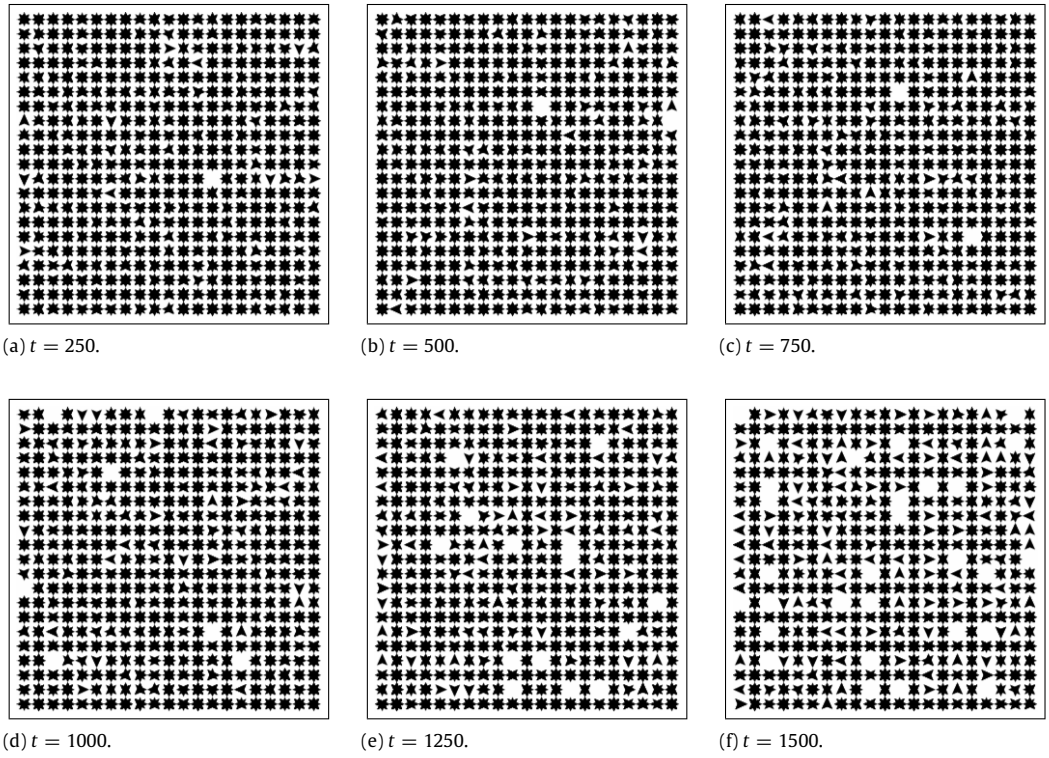

(a) $t = 250$. (b) $t = 500$. (c) $t = 750$.

(d) $t = 1000$. (e) $t = 1250$. (f) $t = 1500$.

Fig. 12. Snapshots of the discrete model with $a = 0.3, b = 0.5$.

detection range is $v^r_{ij} - 1$ and the total number of particles within the detection range in all directions surrounding (i, j) is $v_{ij} - 1$. Similar quantities are defined for the other directions (left, up, and down).

To address the terms in (5), we start by considering the ways for the system to enter the state Ψ with a particle moving right from position (i, j). There are 8 ways in which a right-moving particle from (i, j) will result in entering the given state:

1. A right-moving particle moves out of (i, j) to the right to enter the state Ψ. We assume that in a small time step, only one particle can move at a time and it can only move to a neighboring space. Therefore, the only way this can occur is

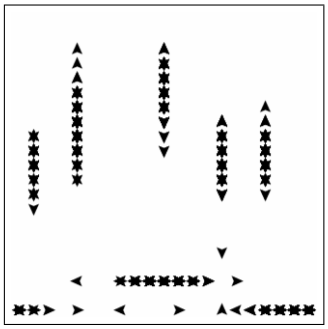

Fig. 13. The discrete model with $a = 0.1$, $b = 0$ advanced to $t = 5000$. Aggregates in both directions are observed.

if there were previously $r_{ij}+1$ right-moving particles at (i,j) and $r_{i+1,j}-1$ right-moving particles at $(i+1,j)$. Since there is one fewer particle at $(i+1,j)$ compared to state Ψ, there are $\nu_{ij}-1$ detectable particles and $\nu^r_{ij}-1$ detectable right-moving particles. There is an additional particle at (i,j), but recall that this is not counted as a detectable particle. Hence, the rate at which these particles could move to the right is the sum of the persistence probability and the neighbor-weight probability, i.e., $a+\overline{c^r_{ij}}$. Accordingly, the probability that a particle moves out of (i,j) to the right to enter the state Ψ is $(a+\overline{c^r_{ij}})(r_{ij}+1)\tilde{P}(r_{ij}+1, r_{i+1,j}-1)$.

2. A left-moving particle moves out of (i,j) by choosing to move to the right: $\overline{c^r_{ij}}(l_{ij}+1)\tilde{P}(l_{ij}+1, r_{i+1,j}-1)$.
3. An up-moving particle moves out of (i,j) by choosing to move to the right: $\overline{c^r_{ij}}(u_{ij}+1)\tilde{P}(u_{ij}+1, r_{i+1,j}-1)$.
4. A down-moving particle moves out of (i,j) by choosing to move to the right: $\overline{c^r_{ij}}(d_{ij}+1)\tilde{P}(d_{ij}+1, r_{i+1,j}-1)$.
5. A right-moving but stationary particle initiates a motion to the right: $(a+\overline{c^r_{ij}})(r^s_{ij}+1)\tilde{P}(r^s_{ij}+1, r_{i+1,j}-1)$.
6. A left-moving and stationary particle moves to the right: $\overline{c^r_{ij}}(l^s_{ij}+1)\tilde{P}(l^s_{ij}+1, r_{i+1,j}-1)$.
7. An up-moving and stationary particle moves to the right: $\overline{c^r_{ij}}(u^s_{ij}+1)\tilde{P}(u^s_{ij}+1, r_{i+1,j}-1)$.
8. A down-moving and stationary particle moves to the right: $\overline{c^r_{ij}}(d^s_{ij}+1)\tilde{P}(d^s_{ij}+1, r_{i+1,j}-1)$.

Combining these eight paths of entering the state Ψ, we obtain

$$\begin{aligned}
&P(\text{Entering state } \Psi \text{ via a particle moving to the right}\\
&\quad\text{into bin}(i,j)) = (a+\overline{c^r_{ij}})(r_{ij}+1)\tilde{P}(r_{ij}+1, r_{i+1,j}-1)\\
&\quad+\overline{c^r_{ij}}(l_{ij}+1)\tilde{P}(l_{ij}+1, r_{i+1,j}-1)\\
&\quad+\overline{c^r_{ij}}(u_{ij}+1)\tilde{P}(u_{ij}+1, r_{i+1,j}-1)\\
&\quad+\overline{c^r_{ij}}(d_{ij}+1)\tilde{P}(d_{ij}+1, r_{i+1,j}-1)\\
&\quad+(a+\overline{c^r_{ij}})(r^s_{ij}+1)\tilde{P}(r^s_{ij}+1, r_{i+1,j}-1)\\
&\quad+\overline{c^r_{ij}}(l^s_{ij}+1)\tilde{P}(l^s_{ij}+1, r_{i+1,j}-1)\\
&\quad+\overline{c^r_{ij}}(u^s_{ij}+1)\tilde{P}(u^s_{ij}+1, r_{i+1,j}-1)\\
&\quad+\overline{c^r_{ij}}(d^s_{ij}+1)\tilde{P}(d^s_{ij}+1, r_{i+1,j}-1). \qquad (6)
\end{aligned}$$

Our goal now is to derive an expression for the expectation of the number of the right-moving particles at node (m,n), r_{mn}. Hence, we multiply (6) by r_{mn} and sum over i, j, and all possible states Ψ.

Assume for simplicity that neither m nor n are 1 or k. We consider the first term in (6), and change variables $r'_{ij} = r_{ij}+1$ and $r'_{i+1,j} = r_{i+1,j}-1$. If $(i,j) \neq (m,n)$ and $(i,j) \neq (m-1,n)$, then (after returning to our original variables) we are left with $r_{mn}(a+c^r_{ij})r_{ij}P$. If $(i,j) = (m,n)$, then we have $(r_{mn}-1)(a+c^r_{mn})r_{mn}P$. If $(i,j) = (m-1,n)$, we get $(r_{mn}+1)(a+c^r_{m-1,n})l_{m-1,n}P$. Therefore, the contribution of first term in (6) is

$$\sum_{i,j,\Psi} r_{mn}(a+c^r_{ij})r_{ij}P - (a+c^r_{mn})r_{mn}P + (a+c^r_{m-1,n})r_{m-1,n}P. \qquad (7)$$

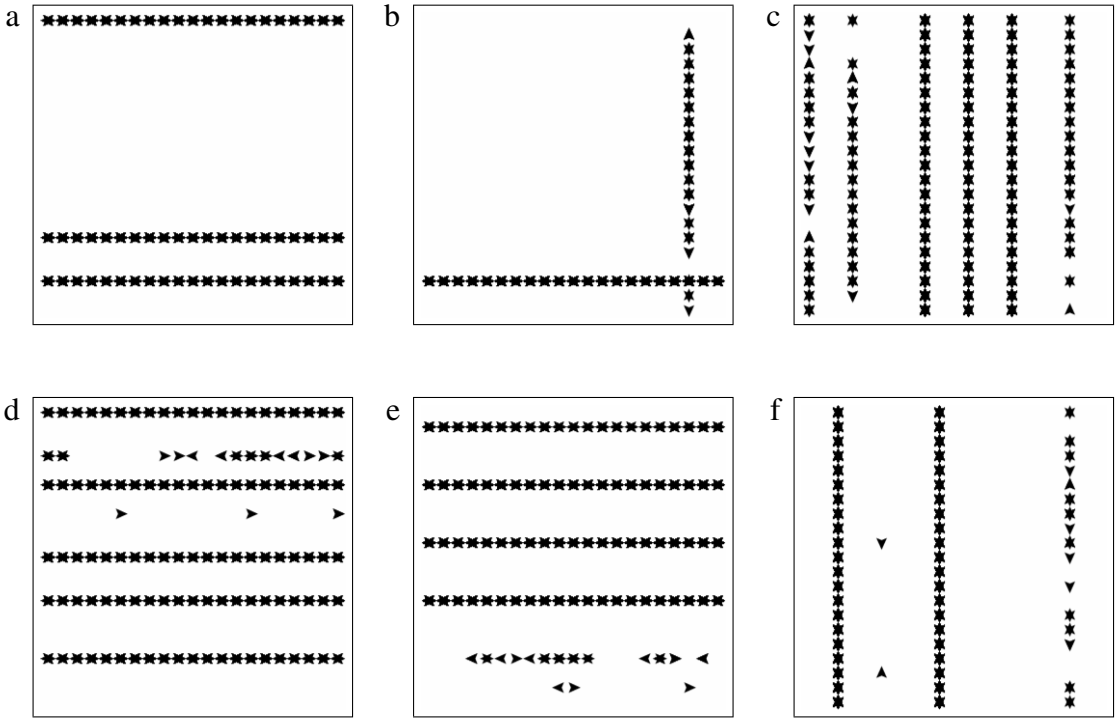

Fig. 14. Various possible outcomes at $t = 1500$ for the same initial condition from Fig. 1. Here, $a = 0.3$, $b = 0.1$.

For the second term in (6): if $(i, j) \neq (m-1, n)$, we get $r_{mn}c^r_{ij}l_{ij}P$, while if $(i, j) = (m-1, n)$, we get $(r_{mn}+1)c^r_{m-1,n}r_{m-1,n}P$. Therefore, the contribution of the second term in (6) is

$$\sum_{i,j,\Psi} r_{mn}c^r_{ij}l_{ij}P + c^r_{m-1,n}l_{m-1,n}P. \tag{8}$$

Similar expressions hold for the other terms in (6).

We now return to (5) and consider ways for the system to leave a state due to a particle moving right. There are 8 ways for the system to leave state Ψ due to the motion of a particle to the right. These can be represented by the following expression:

$$-\left[(a + c^r_{ij})r_{ij}P + c^r_{ij}l_{ij}P + c^r_{ij}u_{ij}P + c^r_{ij}d_{ij}P + (a + c^r_{ij})r^s_{ij}P + c^r_{ij}l^s_{ij}P + c^r_{ij}u^s_{ij}P + c^r_{ij}d^s_{ij}P\right]. \tag{9}$$

The terms in (9) represent a loss for the system, which is the reason for the negative sign. We multiply (9) by r_{mn} and sum over i, j and all states Ψ. After combining the result with the contributions obtained from all terms in (6), we have

$$\begin{aligned}&-\left\langle(a + c^r_{mn})r_{mn}\right\rangle + \left\langle(a + c^r_{m-1,n})r_{m-1,n}\right\rangle + \left\langle c^r_{m-1,n}l_{m-1,n}\right\rangle \\ &+ \left\langle c^r_{m-1,n}u_{m-1,n}\right\rangle + \left\langle c^r_{m-1,n}d_{m-1,n}\right\rangle + \left\langle(a + c^r_{m-1,n})r^s_{m-1,n}\right\rangle \\ &+ \left\langle c^r_{m-1,n}l^s_{m-1,n}\right\rangle + \left\langle c^r_{m-1,n}u^s_{m-1,n}\right\rangle + \left\langle c^r_{m-1,n}d^s_{m-1,n}\right\rangle,\end{aligned} \tag{10}$$

where $\langle x\rangle$ denotes the expectation of x, i.e., $\sum_\Psi xP(\Psi)$. Combining terms multiplied by $c^r_{m-1,n}$ and defining $\eta_{m,n}$ as the sum of all particles at (m, n) (stationary and moving), we can simplify (10) as

$$a\left(\left\langle r_{m-1,n}\right\rangle + \left\langle r^s_{m-1,n}\right\rangle\right) + \left\langle c^r_{m-1,n}\eta_{m-1,n}\right\rangle - \left\langle(a + c^r_{mn})r_{mn}\right\rangle. \tag{11}$$

In order to obtain the ODE for $\langle r_{mn}\rangle$ we have to account for additional items, i.e., the right-moving particles that choose to move in a different direction or become stationary. We omit the details for the sake of brevity. Once all terms are accounted for, the resulting equation becomes

$$\frac{d\langle r_{mn}\rangle}{dt} = a\left(\left\langle r_{m-1,n}\right\rangle + \left\langle r^s_{m-1,n}\right\rangle\right) + \left\langle c^r_{m-1,n}\eta_{m-1,n}\right\rangle - \langle r_{mn}\rangle. \tag{12}$$

We now define $R_{mn} = \langle r_{mn}\rangle, R^s_{mn} = \langle r^s_{mn}\rangle$, and use a similar notation for the other directions. After switching back to i and j as indices, the ODE for right-moving particles reads

$$\frac{dR_{ij}}{dt} = a\left(R_{i-1,j} + R^s_{i-1,j}\right) + \left\langle c^r_{i-1,j}\eta_{i-1,j}\right\rangle - R_{ij}. \tag{13}$$

When i or j is 1 or k, Eqs. (13) are valid with the appropriate adjustments due to the periodic boundary conditions.

Repeating the derivation in all other directions we obtain the system

$$\begin{aligned}\frac{dR_{ij}}{dt} &= a\left(R_{i-1,j} + R^s_{i-1,j}\right) + \left\langle c^r_{i-1,j}\eta_{i-1,j}\right\rangle - R_{ij},\\ \frac{dL_{ij}}{dt} &= a\left(L_{i+1,j} + L^s_{i+1,j}\right) + \left\langle c^l_{i+1,j}\eta_{i+1,j}\right\rangle - L_{ij},\\ \frac{dU_{ij}}{dt} &= a\left(U_{i,j-1} + U^s_{i,j-1}\right) + \left\langle c^u_{i,j-1}\eta_{i,j-1}\right\rangle - U_{ij},\\ \frac{dD_{ij}}{dt} &= a\left(D_{i,j+1} + D^s_{i,j+1}\right) + \left\langle c^d_{i,j+1}\eta_{i,j+1}\right\rangle - D_{ij},\\ \frac{dL^s_{ij}}{dt} &= bL_{ij} - (1-b)L^s_{ij},\\ \frac{dR^s_{ij}}{dt} &= bR_{ij} - (1-b)R^s_{ij},\\ \frac{dU^s_{ij}}{dt} &= bU_{ij} - (1-b)U^s_{ij},\\ \frac{dD^s_{ij}}{dt} &= bD_{ij} - (1-b)D^s_{ij}.\end{aligned} \tag{14}$$

The form of the ODEs in (14) is intuitive. For example, consider the equation for L_{ij}. There are two possibilities for the number of left-moving particles at (i, j) to increase. First, a most recently left-moving particle at $(i + 1, j)$ could continue in its previous direction with probability a. Second, any particle at $(i + 1, j)$ could choose to move to the left with probability $(1 - a - b)$ multiplied by the ratio of particles to the left versus all detectable particles. Also, after an infinitesimal amount of time, all particles at (i, j) have either moved elsewhere or become stationary, hence the $-L_{ij}$ term. Similarly, the form of the equation for L^s_{ij} is also clear: increases occur when left-moving particles become stationary with probability b while decreases occur when stationary particles become non-stationary with probability $1 - b$.

4.2. Simulations

We follow [1] and approximate expectations of quotients and products of random variables by quotients and products of expectations to close the system. We would like to see how the ODE model compares to an ensemble average of the discrete model. First, we randomly place 1000 particles on an 11×11 grid and assign each particle a memory in the form of its last direction of motion, with equal probabilities for each direction. These initial conditions are then used for simulating the dynamics of both models. We then run the simulations until the configuration reaches a steady state ($t = 1000$ for the ODE model and $t = 500$ for the stochastic particle model). The stochastic particle model is run in NetLogo and the ODE model is run in Matlab using ODE45 with default parameters. We run the stochastic model 5000 times and average over all simulations. The results are shown in Fig. 15 for a variety of a and b values.

We note that there are both similarities and differences between the ODE and averaged results. In Fig. 15(a)–(c), the ODEs generate a few aggregates that increase in length as a increases, as observed in the discrete model simulations. Most of these aggregates can also be seen in the corresponding ensemble average, but the number of particles found in these positions is much smaller, as the averaging procedure causes the particles to be more spread out. In addition, the averaged pictures have aggregates where no aggregates appear from the ODEs. For instance, in Fig. 15(b) and (c), we have both horizontal and vertical aggregates on the right side, but only horizontal aggregates on the left. We have seen that, except for small values of the parameters, only purely horizontal or vertical aggregates arise. The ODEs, therefore, seem to give results comparable to an individual realization of the model, rather than an average. We also note that in Fig. 15(d), the ODEs show little variation in the number of particles found in each position. We discuss this further below.

We now proceed to simulate the ODE model in different setups. We initialize the system by taking the number of left, right, up, and down moving particles on each position to be Poisson with mean 2. We assume no stationary particles initially. Fig. 16 shows a time series of the ODE model on a 50×50 grid with 20 208 particles. By time $t = 100$, distinct aggregates have begun to form. As time progresses, aggregates coalesce and become more Gaussian.

Fig. 17 shows the results obtained at $t = 1000$ when $b = 0$ and $a \in \{0.1, 0.2, 0.3, 0.4\}$. For $a = 0.1$, many small peaks form. For $a = 0.2$, we have fewer and broader peaks. Gaussian behavior is apparent for $a = 0.3$. Finally, for $a = 0.4$, there are no aggregates; this demonstrates a breakdown in the ODEs when the parameters become too large. It may be this behavior that is linked to the loss of preferential locations for aggregates to form in the discrete model.

In Fig. 18 we fix $b = 0.1$ and vary a. Results are shown at $t = 1000$. There is no significant difference between the results shown in Fig. 18 and those that were shown in Fig. 17. The only noticeable

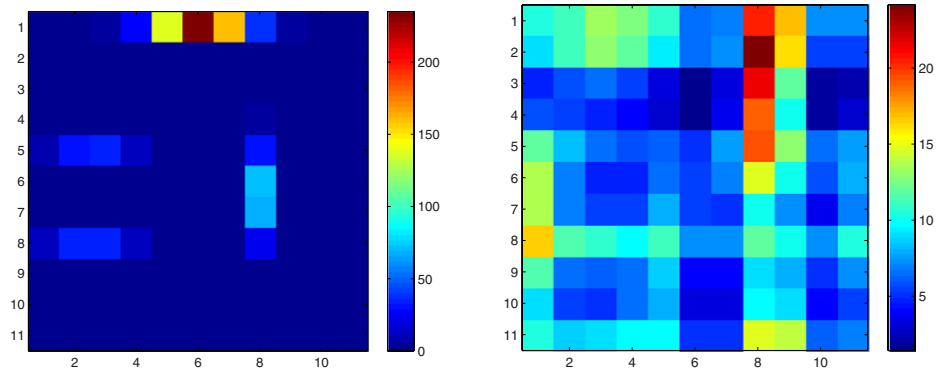

(a) $a = 0.1, b = 0.1$.

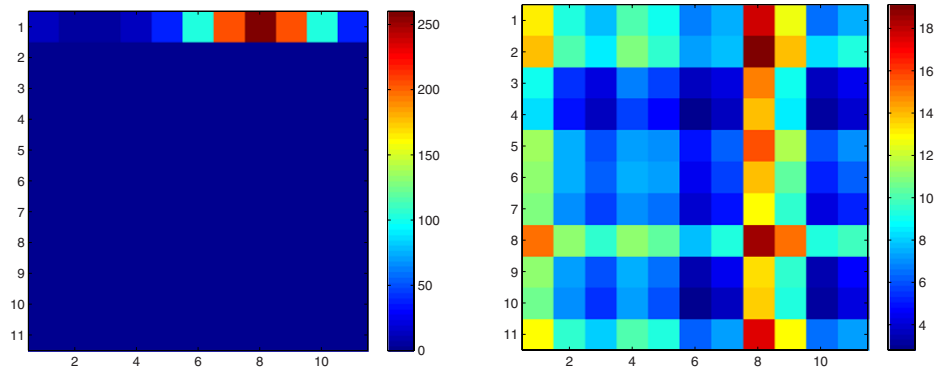

(b) $a = 0.2, b = 0.1$.

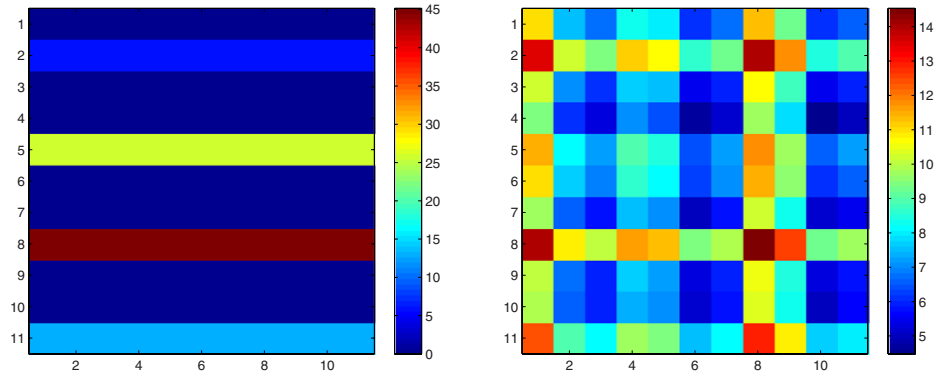

(c) $a = 0.3, b = 0.1$.

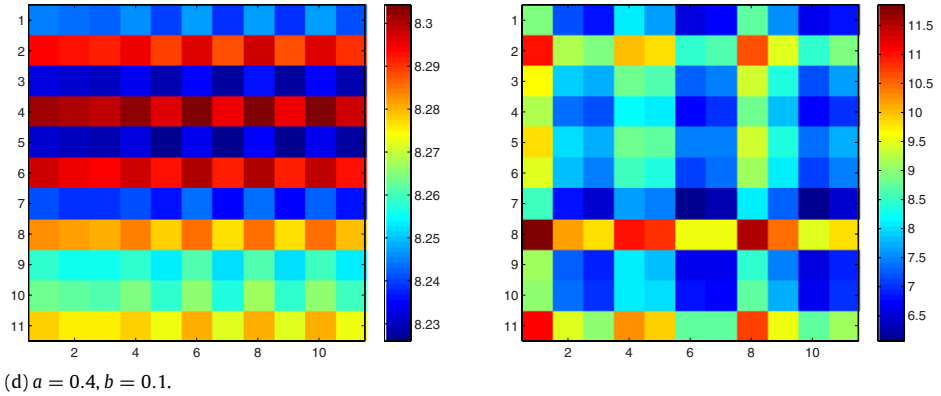

(d) $a = 0.4, b = 0.1$.

Fig. 15. Comparisons between the ODE model (left) and the stochastic model averaged over 5000 runs (right).

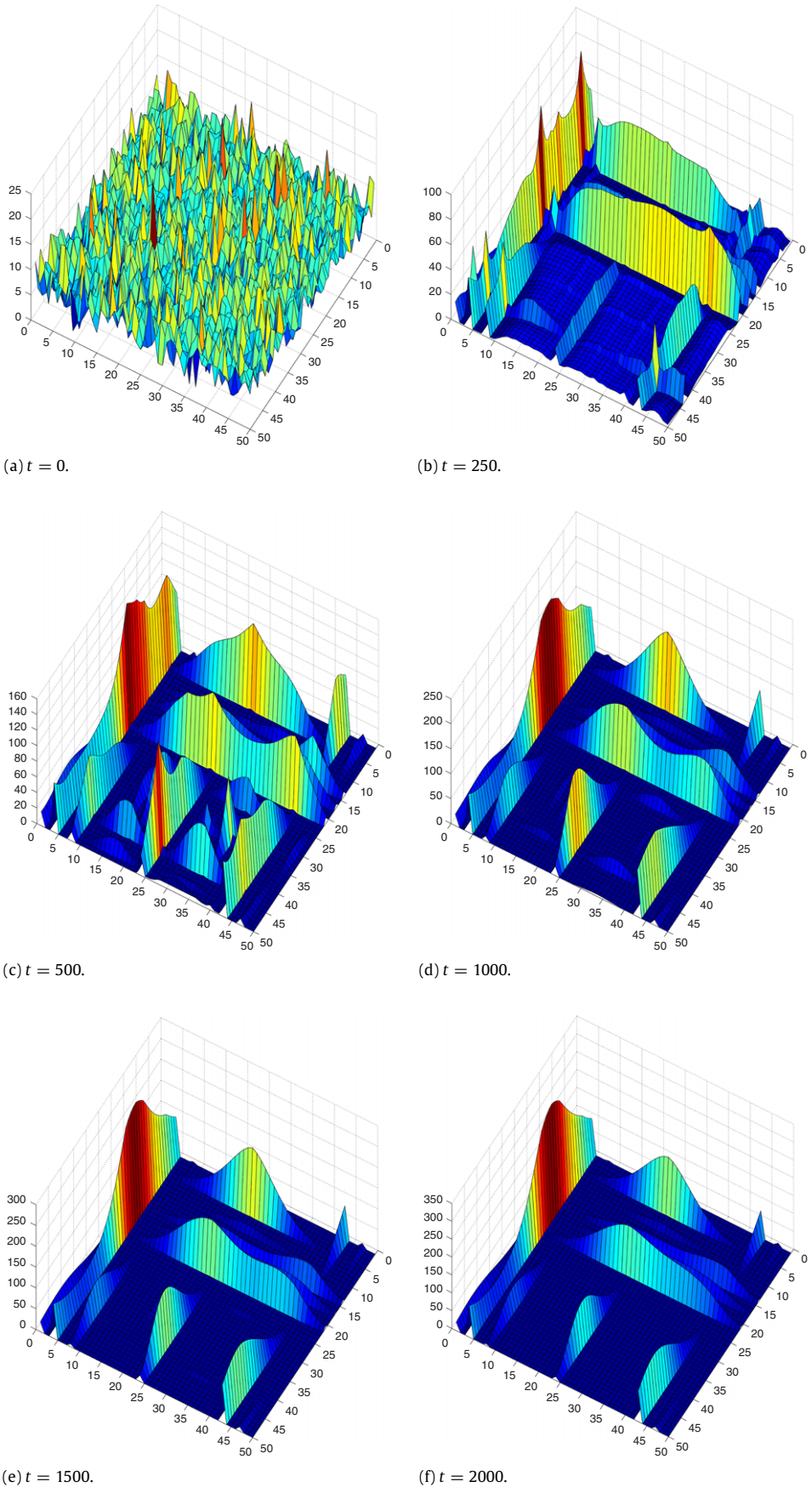

(a) $t = 0$. (b) $t = 250$.

(c) $t = 500$. (d) $t = 1000$.

(e) $t = 1500$. (f) $t = 2000$.

Fig. 16. Time evolution of ODE with $a = 0.3$, $b = 0$ on a 50×50 grid.

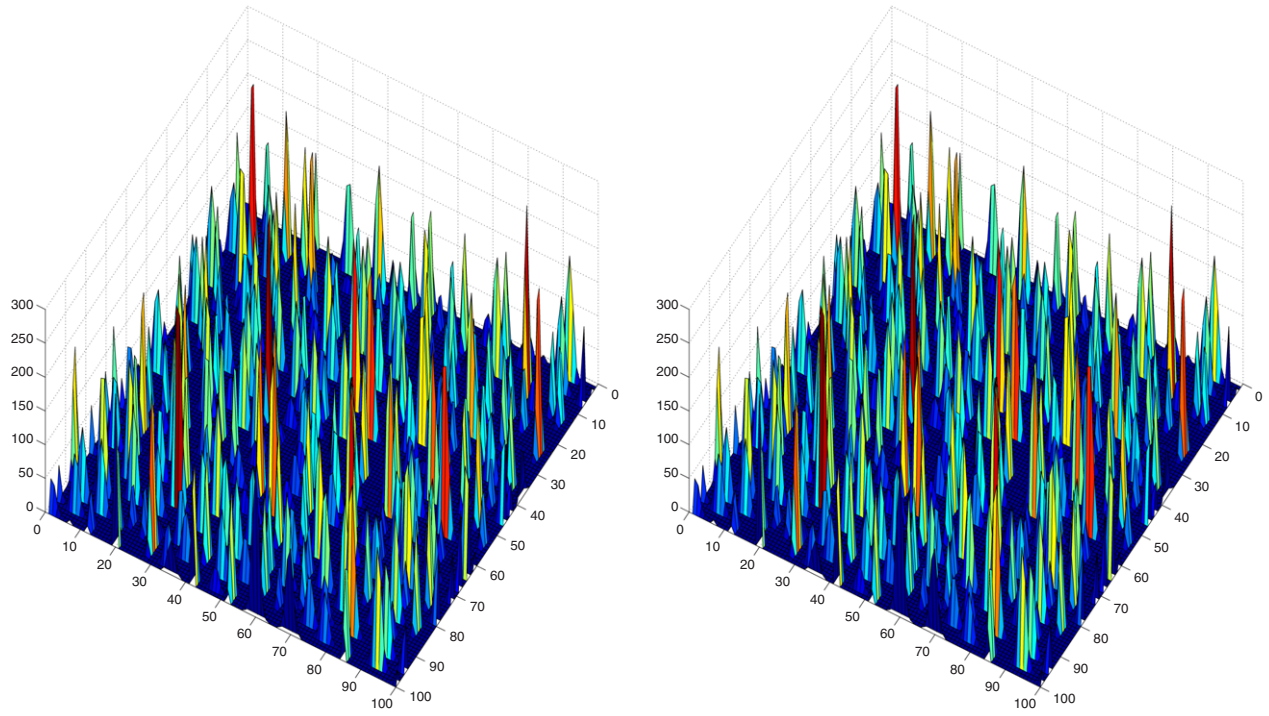

(a) $a = 0.1, b = 0$.

(b) $a = 0.2, b = 0$.

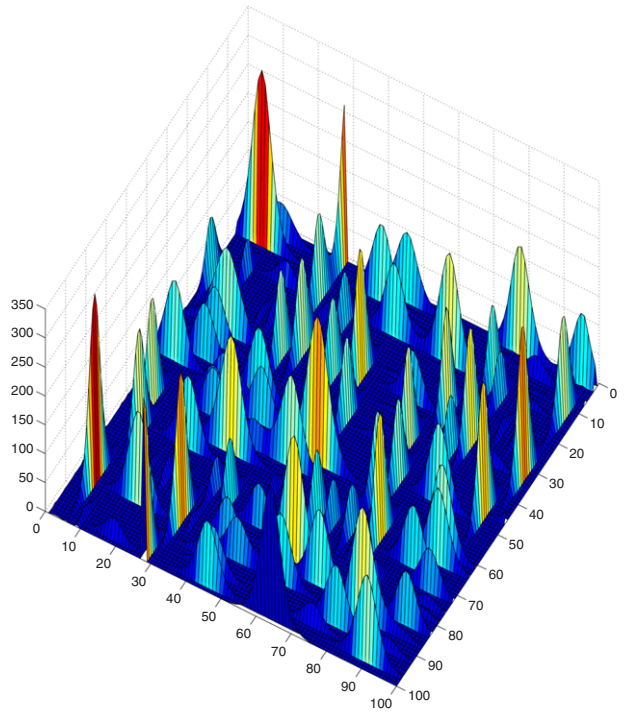

(c) $a = 0.3, b = 0$.

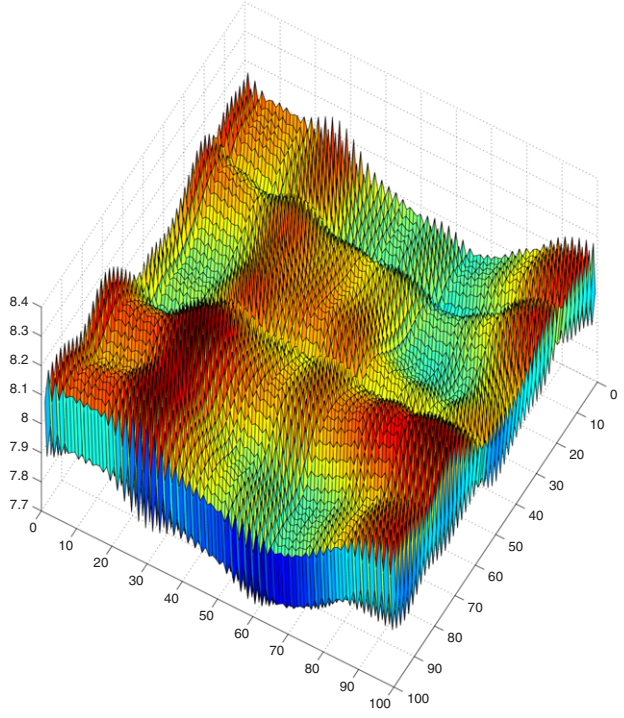

(d) $a = 0.4, b = 0$.

Fig. 17. Results from the ODE model at $t = 1000$ for $b = 0$ and $a = 0.1, 0.2, 0.3, 0.4$.

difference is that Fig. 18(c) contains non-Gaussian aggregates. In fact, if we run the simulation for a longer time, Gaussian-type aggregates emerge. This is shown in Fig. 19 for time $t = 2000$. Such aggregates take longer time to form due to the nonzero value of the probability to remain stationary b.

The simulations shown so far suggest that the only types of long-term behavior we get are Gaussian or random. However, this is not the case: for example, if we let $(a, b) = (0.35, 0)$, we always have non-Gaussian behavior no matter how long we run the simulation (see Fig. 20). As demonstrated on the 11×11 grid, what we are seeing in the ODE simulations is reminiscent of an individual simulation rather than an ensemble average. Accordingly, simulations of the discrete model on the larger grid also show the same patterns: horizontal and vertical aggregates that coexist at large times, whose lengths increase with a, and with the number of particles in each bin decreasing with their distance from the middle of their aggregate.

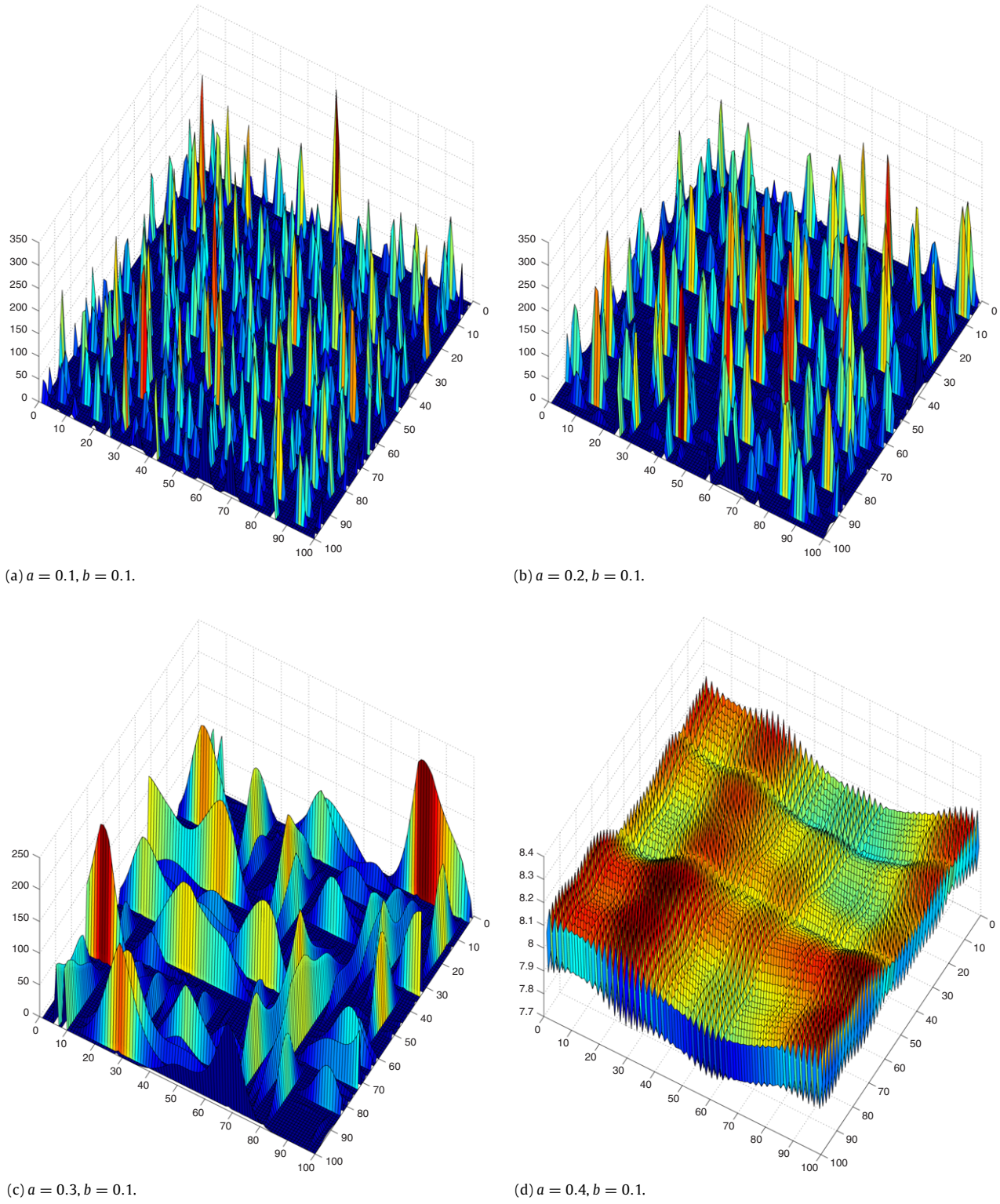

(a) $a = 0.1, b = 0.1$.

(b) $a = 0.2, b = 0.1$.

(c) $a = 0.3, b = 0.1$.

(d) $a = 0.4, b = 0.1$.

Fig. 18. Results from the ODE model at $t = 1000$ for $b = 0.1$ and $a = 0.1, 0.2, 0.3, 0.4$.

By running simulations for many more choices of parameters, we discover that whether aggregates form, does not depend solely on the value of $a + b$. For example, aggregates form for $(a, b) = (0.2, 0.2)$ but not for $(0.4, 0)$. Nevertheless, there does appear to be a constraint on some linear combination of the parameters. To find this constraint, we note that aggregates form for $a = 0$ and any $0 \leq b < 1$. In some cases, we have numerical problems solving the ODE with $a = 0$ for large times, so instead we stop these simulations at $t = 100$. We also note that aggregates form for $(a, b) = (0.367, 0)$, but not for $(0.368, 0)$. Hence, we hypothesize an approximate constraint for aggregate formation as $a/.368 + b < 1$. This constraint accurately predicts aggregate formation in every instance when we vary both a and b over the set $\{0, 0.1, 0.2, \ldots, 1\}$ (see Fig. 21). In addition, the constraint correctly predicts that aggregates do not form for $(a, b) = (0.3, 0.19)$ but do form for $(0.3, 0.182)$ (see Fig. 22).

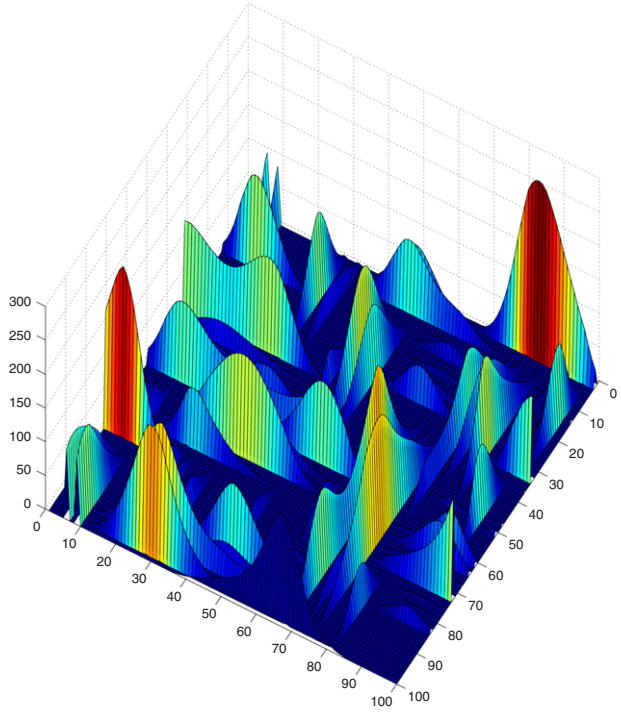

Fig. 19. Results from the ODE model at $t = 2000$ for $a = 0.3$, $b = 0.1$.

In order to test whether this constraint depends on the specific initial conditions, we rerun the above calculations with new Poison-distributed initial conditions. We find that the same approximate constraint holds true for these cases as well, even if we alter the mean of the distribution. We also checked whether the constraint depends on the specific distribution used to generate the initial conditions. Choosing the distribution to be uniform on $\{0, 1, 2, \ldots, 8\}$ led to a similar constraint with a slightly different constant, $a/.357 + b < 1$.

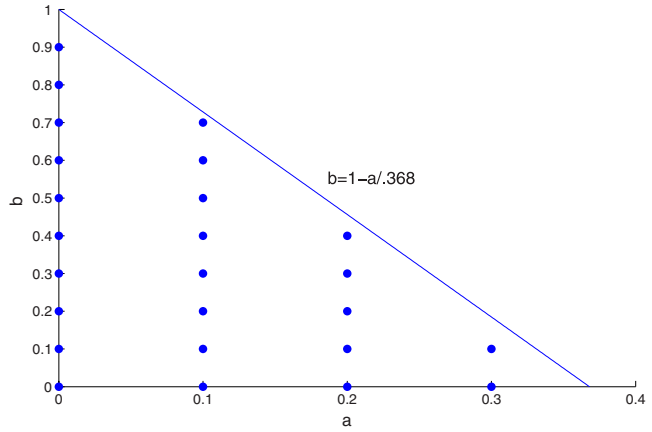

Fig. 21. The region of parameter space for which aggregates form in the ODE model. The model was run, varying a and b over $\{0, 0.1, 0.2, \ldots, 1\}$. The dark circles represent parameter values for which aggregates form. The constraint line is provided for reference.

5. Conclusions

In this paper we generalized the one-dimensional model of Galante and Levy [1] to two dimensions. At every time step particles may persist their motion in their current direction with probability a, remain stationary with probability b, or move toward one of their neighboring particles with equal probabilities. Since there are no exclusion principles in place, multiple particles are allowed to occupy every spot on the lattice, and hence when a particle changes its direction of motion, the new direction is chosen based on a probability that is proportional to the fraction of the neighboring particles in any given direction.

All simulations demonstrated that the limit pattern that emerges is a collection of vertical and/or horizontal aggregates. The lengths of the aggregates increases with the persistence probability a. This can be explained by the fact that aggregates can only

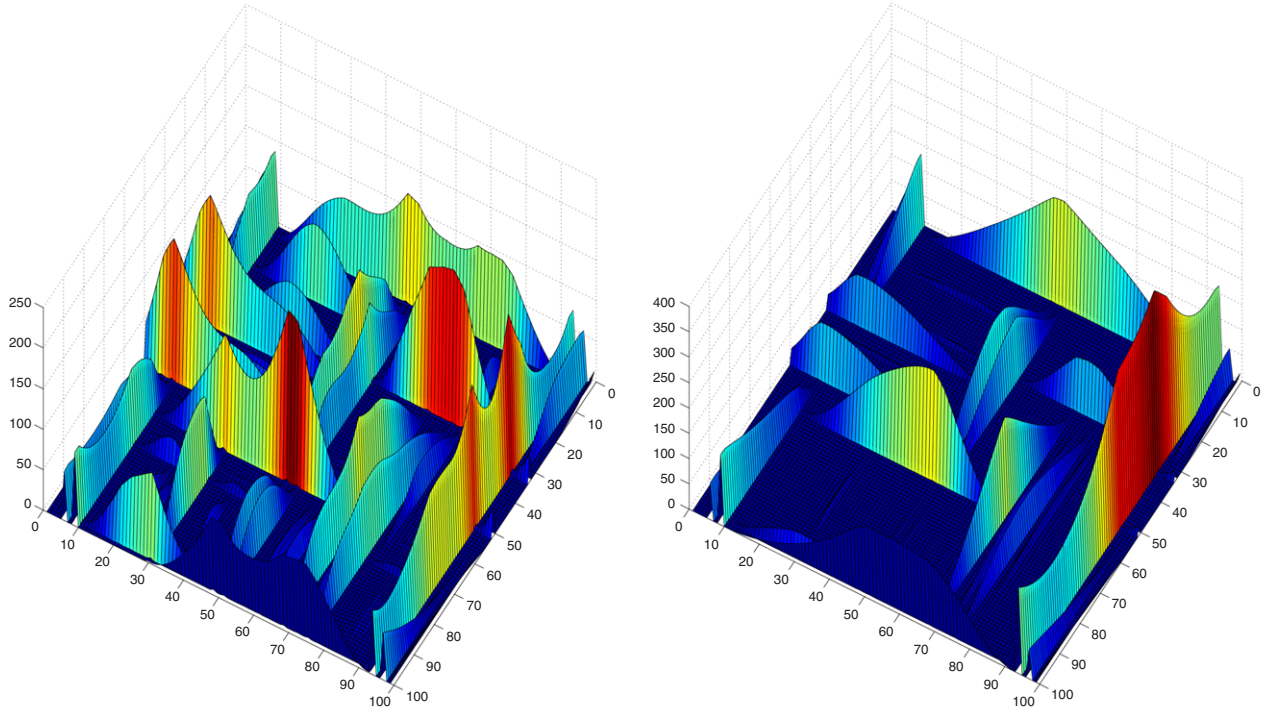

(a) $t = 1000$. (b) $t = 5000$.

Fig. 20. Results from the ODE model at $t = 1000$ and 5000 for $a = 0.35$, $b = 0$.

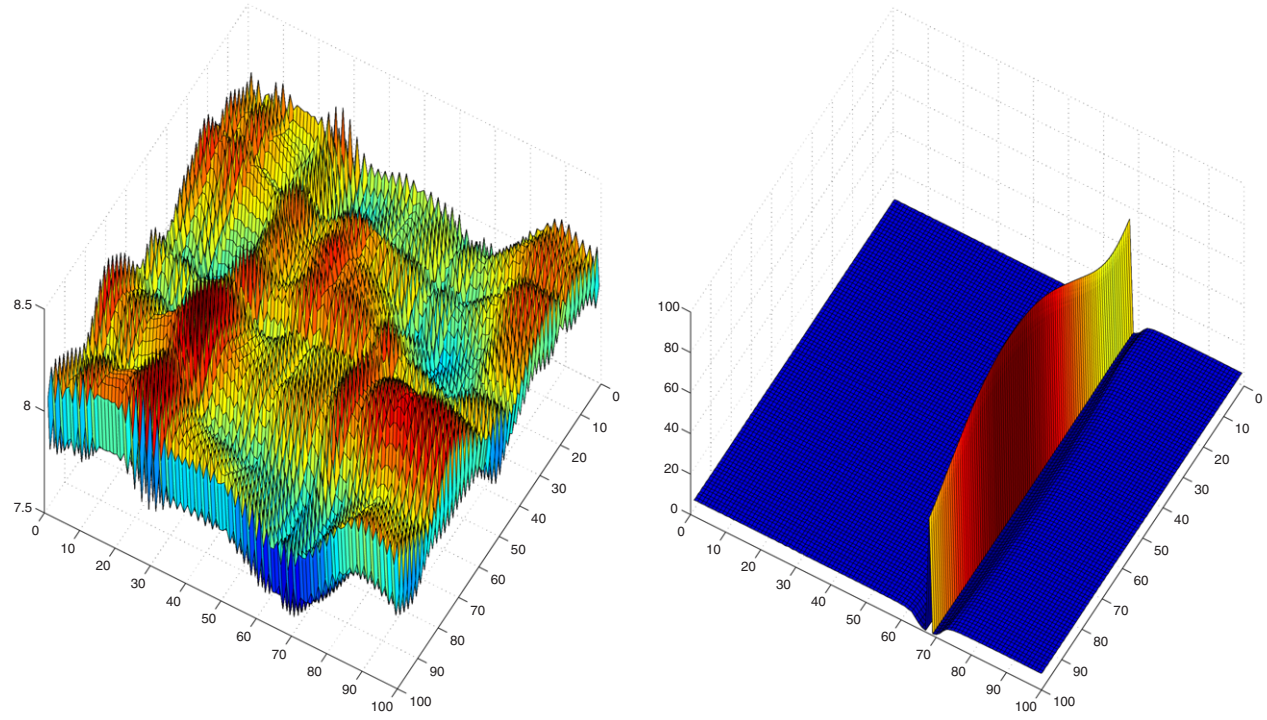

(a) $a = 0.3, b = 0.19$. (b) $a = 0.3, b = 0.182$.

Fig. 22. Demonstration that the constraint accurately predicts the lack of aggregates for $(a, b) = (0.3, 0.19)$ and the existence of aggregates for $(0.3, 0.182)$.

increase in length when a particle on the aggregate edge persists, which is unlikely for small a. When a is fixed and the probability to remain stationary b varies, we note again the emergence of aggregates, the number of which steadily decreases as time elapses and aggregates coalesce. This occurs more rapidly for small values of b as expected. Our simulations suggest that we will always be left with purely vertical or horizontal aggregates if the simulations are run for a sufficiently long time, assuming there is a non-zero probability of particles moving towards their neighbors and the parameters are not too small.

The discrete system was followed by a system of ODEs that was derived in order to capture the time evolution of the expected number of particles. Since this requires us to estimate expectations of products and quotients by products and quotients of expectations, we run Monte Carlo simulations of the discrete model to compare to the ODE results. Though quantitatively different, the ODE model captures much of the behavior seen in individual runs of the particle model. We then run the ODE model for fixed b and varying a. As in the discrete simulations, we obtain aggregates whose lengths increase with a. Unlike the discrete simulations, the ODEs transition into randomness when a linear combination of the parameters becomes too large. This raises some questions including: Why does this transition occur? Why is the constraint linear? Why is the constraint largely unaffected by the initial conditions, including the particular distribution used? These questions can form the topic of further study.

While the derivation of the model was motivated by a biological problem, it is likely that similar models can be applied in other setups. While many models were written in order to describe aggregation patterns, there are very few examples of mathematical models which involve a discrete selection process (in our case, in terms of selecting the direction of motion). It is more common to write models in which the selection process is conducted in some averaged sense, e.g., using some mean field approximations. A unique feature of this model is that while aggregation patterns emerge sooner or later, they are never in steady state: aggregate positions solidify after enough time has passed, but particles continue to move within their aggregates. Most importantly, given the memory that is embedded in the system (in the form of the last direction of motion), stationary particles can restart their motion and drift away from an aggregate.

Acknowledgments

This work was supported in part by the joint NSF/NIGMS program under Grant Number DMS-0758374 and in part by Grant Number R01CA130817 from the National Cancer Institute. The content is solely the responsibility of the authors and does not necessarily represent the official views of the National Cancer Institute or the National Institutes of Health.

References

[1] A. Galante, D. Levy, Modeling selective local interactions with memory, Physica D (2012) http://dx.doi.org/10.1016/j.physd.2012.10.010.
[2] A. Galante, S. Wisen, D. Bhaya, D. Levy, Modeling local interactions during the motion of cyanobacteria, J. Theoret. Biol. 309 (2012) 147–158.
[3] A. Galante, S. Wisen, D. Bhaya, D. Levy, Stochastic models and simulations of phototaxis, in: H. Sayama, A.A. Minai, D. Braha, Y. Bar-Yam (Eds.), Unifying Themes in Complex Systems Volume VIII: Proceedings of the Eighth International Conference on Complex Systems, in: New England Complex Systems Institute Series on Complexity, NECSI Knowledge Press, Boston, MA, 2011, pp. 105–119.
[4] S.-Y. Ha, D. Levy, Particle, kinetic, and fluid models for phototaxis, Discrete Contin. Dyn. Syst. Ser. B 12 (2009) 77–108.
[5] D. Levy, T. Requeijo, Modeling group dynamics of phototaxis: from particles to PDEs, Discrete Contin. Dyn. Syst. Ser. B. 9 (2008) 108–128.
[6] D. Levy, T. Requeijo, Stochastic models for phototaxis, Bull. Math. Biol. 70 (2008) 1684–1706.
[7] D. Bhaya, Light matters: phototaxis and signal transduction in unicellular cyanobacteria, Mol. Microbiol. 53 (2004) 745–754.
[8] M. Burriesci, D. Bhaya, Tracking phototactic responses and modeling motility of synechocystis sp. Strain PCC6803, J. Photochem. Photobiol. B 91 (2008) 77–86.
[9] R.E. Baker, C.A. Yates, R. Erban, From microscopic to macroscopic descriptions of cell migration on growing domains, Bull. Math. Biol. 72 (2010) 719–762.
[10] I. Aoki, A simulation study on the schooling mechanism in fish, Bull. Japan Soc. Sci. Fisher. 48 (8) (1982) 1081–1088.

[11] T. Oboshi, S. Kato, A. Mutoh, H. Itoh, A simulation study on the form of fish schooling for escape from predator, Forma 18 (2003) 119–131.
[12] J.K. Parrish, S.V. Viscido, D. Grunbaum, Self-organized fish schools: an examination of emergent properties, Biol. Bull. 202 (2002) 296–305.
[13] S. Stöcker, Models for tuna school formation, Math. Biosci. 156 (1999) 167–190.
[14] F. Cucker, S. Smale, Emergent behavior in flocks, IEEE Trans. Automat. Control 52 (2007) 852–862.
[15] C.W. Reynolds, Flocks, herds, and schools: a distributed behavioral model, Proc. Comput. Graphics, ACMSIGGRAPH87 Conf. 21 (1987) 25–34.
[16] T. Ikawa, H. Okabe, Three-dimensional measurements of swarming mosquitoes: a probabilistic model, measuring system, and example results, in: Parish, Hamner (Eds.), Animal Groups in Three Dimensions, Cambridge, 1997.
[17] A. Okubo, H.C. Chiang, An analysis of the kinematics of swarming of anarete pritchardi kim (diptera: cecidomyiidae), Res. Popul. Ecol. 16 (1974) 1–42.
[18] T. Vicsek, A. Czirk, E. Ben-Jacob, I. Cohen, O. Shochet, Novel type of phase transition in a system of self-driven particles, Phys. Rev. Lett. 6 (1995) 1226–1229.
[19] I.D. Couzin, J. Krause, R. James, G.D. Ruxton, N.R. Franks, Collective memory and spatial sorting in animal groups, J. Theoret. Biol. 218 (2002) 1–11.